4D in vivo quantification of ankle joint space width using dynamic MRI

K. Makki, B Borotikar, M Garetier, Oscar Acosta, S Brochard, D Ben Salem, François Rousseau

4D in vivo quantification of ankle joint space width using dynamic MRI

K. Makki[1,*] , B. Borotikar[2], M. Garetier[3], O. Acosta[4], S. Brochard[2], D. Ben Salem[2], F. Rousseau[1]

***Abstract*— Spatio-temporal evolution of joint space width (JSW) during motion is of great importance to help with making early treatment plans for degenerative joint diseases like osteoarthritis (OA). These diseases can affect people of all ages leading to an acceleration of joint degeneration and to limitations in the activities of daily living. However, only a few studies have attempted to quantify the JSW from moving joints. In this paper, we present a generic pipeline to accurately determine the changes of the JSW during the joint motion cycle. The key idea is to combine spatial information of static MRI with temporal information of low-resolution (LR) dynamic MRI sequences via an intensity-based registration framework, leading to a high-resolution (HR) temporal reconstruction of the joint. This allows the temporal JSW to be measured in the HR domain using an Eulerian approach for solving partial differential equations (PDEs) inside a deforming inter-bone area where the HR reconstructed bone segmentations are considered as temporal Dirichlet boundaries. The proposed approach has been applied and evaluated on *in vivo* MRI data of five healthy children to non-invasively quantify the spatio-temporal evolution of the JSW of the ankle (tibiotalar joint) during the entire dorsi-plantar flexion motion cycle. Promising results were obtained, showing that this pipeline can be useful to perform large-scale studies containing subjects with OA for different joints like ankle and knee.**

***Index Terms*— Dynamic MRI, intensity-based registration, joint space width (JSW), partial differential equations (PDEs).**

I. INTRODUCTION

Providing accurate spatial-temporal information on the JSW can help researchers and clinicians in identifying the critical phases of movement and making early treatment plans for degenerative joint diseases like OA. In the literature, most studies were based on stationary acquisitions from different joints to evaluate intra-subject (over a large period of time) [1] or inter-subject variability of the JSW [2]. In [3], *Goker et al.* quantified the tibiotalar JSW using 2D radiographic examinations. However, 2D measures are typically less informative than 3D measures simply because the human joints are complex 3D structures. In [4], the authors evaluated the tibiotalar JSW using 3D reconstruction of *stationary* CT images. However, their study reports only results at three specific locations (neutral position, maximum dorsiflexion, and maximum plantar flexion of the ankle joint) in addition to the invasive nature of X-ray radiation.

Recently, *Borotikar et al.* [5] proposed a method to quantify patellofemoral cartilage contact kinematics based on the overlap between the two contact cartilage layers under the assumption that each cartilage layer should undergo the same rigid transform as that of the attached bone. However, it was needed to manually segment the dynamic data as they used mesh-based registration for reconstructing HR temporal bone models. Moreover, this manual intervention is time consuming and prone to segmentation bias because of noise and low-resolution of dynamic data. Another limitation of this method is that it offers limited spatial information (only overlapped regions are highlighted). In summary, tracking the entire joint space area and performing accurate measures of the JSW throughout a specific joint trajectory are still challenging because articular cartilages undergo non-linear deformations during motion. In the context of soft-tissue thickness quantification, *Yezzi et al.* [6] presented an Eulerian framework for computing the thickness of tissues based on the solution of Laplace's equation between two simply connected boundaries. These techniques have been successfully employed to measure the cortical thickness [7] and to segment the articular cartilages from conventional MRI of the knee joint [8]. In this paper, we extend these techniques to the measurement of the JSW during the entire joint motion cycle using dynamic MRI sequences, which will certainly provide new temporal motion features. In our previous work [9], we have proposed a motion-based algorithm for estimating HR dynamic MRI sequences via a log-euclidean polyrigid framework (LEPF) [10] using both static and dynamic MRI. In the current work, we use the associated motion estimation algorithm to track the tibiotalar joint with high accuracy and without the need for manual segmentation of dynamic data. The main goal is to identify the spatial location of each bone and of the joint space section at each time frame, but in the HR domain of the static scan (*i.e.* image resolution of $0.26 \times 0.26 \times 0.8mm$). So that the temporal JSW measures are performed in this HR domain.

To summarize, we present a complete pipeline for : 1) estimating spatio-temporal bone rigid transformations (Section III-A), 2) computing spatio-temporal non-rigid deformations of the joint space area using the LEPF (Section III-B), 3) measuring dynamic, *in vivo* JSW via an iterative relaxation method (3) using the high-resolution-reconstructed bone segmentations as Dirichlet boundaries (Section III-C).

II. MRI SCANNING

Data were acquired as part of a pilot study for five healthy children (range 10–14 years) at CHRU of Brest, France, under a protocol approved by the Institutional Review Board (IRB). Children were selected with no contraindications to MRI and with no history of lower limb musculo-skeletal

*This work was supported by Région Bretagne, Chaire d'excellence INSERM-IMT Atlantique, Fondation de l'Avenir, and Fondation Motrice.

[1]IMT Atlantique, LaTIM U1101 INSERM, UBL, Brest, France
[2]UBO, LaTIM U1101 INSERM, CHRU Brest, Brest, France
[3]HIA Brest, LaTIM U1101 INSERM, Brest, France
[4]Univ Rennes, LTSI - UMR 1099 INSERM, Rennes, France

injury or surgery in the past six months in order to establish normative contact mechanics before focusing on pathomechanics studies. HR images of the ankle were obtained using a 3D T1-weighted GE sequence (TR= $7.81ms$, TE= $2.75ms$, FA= $10°$, FOV $150mm \times 150mm$, voxel size of $0.26 \times 0.26 \times 0.8mm$, and matrix 576×576), using a 3T clinical MR imaging scanner (Achieva dStream, Philips Medical Systems, Best, NL). Ankle passive movements were standardized for all subjects using a specifically designed orthotic fixture in order to perform coherent averaging of the results. Real-time FFE (Fast Field Echo) sequences have been acquired to reduce the dynamic-scanning time to 18 sec for a single cycle of dorsi-plantar flexion where motion was consistent and continuous during scanning. With TR= $20.61ms$, TE= $1.8ms$, FA= $15°$, resolution of $0.57 \times 0.57 \times 8mm$, FOV $200mm \times 200mm$, 6 slices per time frame (15 time frames per sequence) and matrix 352×352.

III. Methods

A. Bone motion estimation

The proposed algorithm for bone motion tracking consists in estimating the rigid transformation of each bone between the HR static image and each LR dynamic image. This leads to a high-resolution temporal reconstruction of the ankle joint from LR dynamic MRI sequence. This algorithm require only the manual segmentations of bones of interest in the high-resolution static image as inputs. For more details about this algorithm, the reader is referred to our previous works [9], [11].

B. Temporal tracking of joint space area

Following previous works [3], [4], we define the tibiotalar joint space in healthy feet as the space between the upper surface of the talus and the inferior articular surface of the tibia. The joint space area is manually segmented in the static image (figure 1) and then automatically tracked throughout the dynamic sequence using non-rigid registration. In this work, we propose to compute the local spatio-temporal deformations of this area using the LEPF. The segmentations of the two bones, composing the joint of interest, are used to compute the spatial weighting functions $\{w^i(x)\}_{i\in\{1,2\}}$. The use of this bijective framework ensure the estimation of a smooth and invertible transformation at each voxel x inside the joint space section R_s by integrating its trajectories (from the static image S to each k^{th} time-frame D_k) in the domain of matrix logarithms, via the following equation :

$$\mathcal{T}_{S\rightarrow D_k}(x) = \exp\left(\tilde{w}^1_S(x).\log(\mathrm{T}^1_k) + \tilde{w}^2_S(x).\log(\mathrm{T}^2_k)\right).x \quad (1)$$

where : T^i_k is the rigid transform from S to D_k for the bone i ; $\tilde{w}^i_S(x)$ is the normalized weighting function for the bone i in S (*i.e.* $\tilde{w}^1_S(x) + \tilde{w}^2_S(x) = 1 \forall x \in R_s, R_s \subset S$). To compute the exponential mapping of Equation 1 in regular grids with high-accuracy, we propose to use the matrix eigen-decomposition* instead of the classical use of the scaling and squaring method involving approximation theory where the accuracy always remains debatable [10].

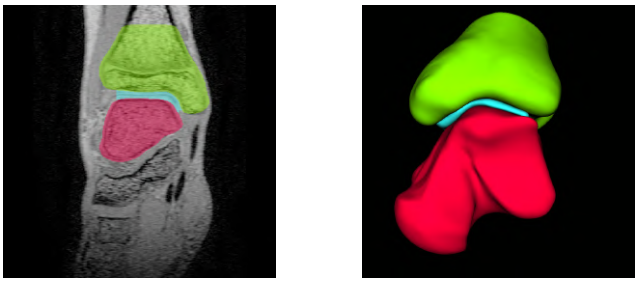

Fig. 1: Segmentation of the tibiotalar joint. Regions of interest are : tibia (green), talus (red), tibiotalar joint space (cyan). From left to right : Mid-coronal image from the HR static image ; 3D rendering of the joint.

C. Computation of temporal joint space width

Given the position of each bone (B^1_k and B^2_k) and each joint space area (R_k) at each time frame D_k, the time-dependent width of the area separating two neighboring bones can be computed with high accuracy using an Eulerian PDE approach [6]. The JSW is computed by first solving Laplace's equation ($\triangle u_k = 0$) inside R_k. For this, we have used the following *Jacobi iterative* method which is simple to implement and numerically robust :

$$u^{i+1}_k(x,y,z) = \tfrac{1}{6}[u^i_k(x+1,y,z) + u^i_k(x-1,y,z) + u^i_k(x,y+1,z) + u^i_k(x,y-1,z) + u^i_k(x,y,z+1) + u^i_k(x,y,z-1)] \quad (2)$$

where $u^i_k(x,y,z)$ is the potential of the point $p = (x,y,z) \in R_k$ during the i^{th} iteration. Bones are considered as Dirichlet boundaries so that they are set to fixed potentials ($u_k(B^1_k) = 0V$ for the inner boundary and $u_k(B^2_k) = 100V$ for the outer boundary). The potential is set to zero at all grid points outside the joint segmentation (including R_k) to connect the two boundaries as shown in figure 5.a in such a way that these values will serve as inner boundary condition. Solving this second order PDE gives the harmonic interpolant u_k which divides R_k into a set of equipotential sub-layers (figure 5.a). Figure 2 shows the solution of Laplace's equation inside a synthetic sphere using the Jacobi iterative method (2).
The normalized gradient vector field $\vec{N}_k = \frac{\nabla u_k}{\|\nabla u_k\|}$ is then computed from u_k with 3D finite differences. From this normalized gradient vector flow, it is then possible to compute the two correspondence trajectories between p and each of the two boundaries, that we note L^0_k and L^1_k, by solving a pair of PDEs in a parallel way : $\nabla L_0.\vec{N} = -\nabla L_1.\vec{N} = 1$. To simplify notations, we denote $L_0 = L^0_k$, $L_1 = L^1_k$, and $\vec{N} = \vec{N_k}$. In this work, L_0 and L_1 are first initialized to $-\frac{(dx+dy+dz)}{6}$ at all grid points and then iteratively *updated* only over R_k using a fast *Gauss-Seidel* method* :

$$\begin{aligned} L^{i+1}_0[x,y,z] &= \tfrac{1}{|N_x|+|N_y|+|N_z|}.(1 + |N_x|\, L^i_0[x \mp 1,y,z] + \\ &\quad |N_y|\, L^i_0[x,y \mp 1,z] + |N_z|\, L^i_0[x,y,z \mp 1]) \\ L^{i+1}_1[x,y,z] &= \tfrac{1}{|N_x|+|N_y|+|N_z|}.(1 + |N_x|\, L^i_1[x \pm 1,y,z] + \\ &\quad |N_y|\, L^i_1[x,y \pm 1,z] + |N_z|\, L^i_1[x,y,z \pm 1]) \end{aligned} \quad (3)$$

where : dx, dy, and dz are the voxel spacing values in the x, y and z directions, respectively ; $m \pm 1 = m + sgn(N_m)$,

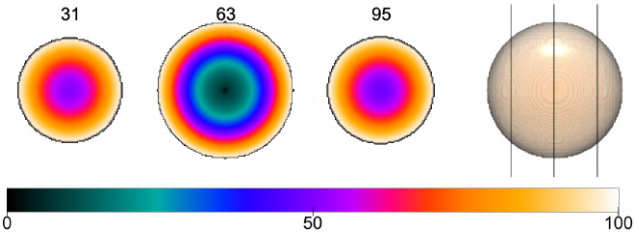

Fig. 2: 3D solution of the Laplace equation u inside a synthetic sphere S (*i.e.* between its center c and its surfaces) using the Jacobi iterative method. The initial Dirichlet boundary conditions are set as follows : $u(c) = 0$ and $u(\bar{S}) = 100$. Three coronal slices are presented to show the harmonic interpolant inside S. From another physical point of view, this can be interpreted as the heat propagation from the outer surface to the sphere center as the Laplace equation is a particular case of the Heat equation.

$m \mp 1 = m - sgn(N_m)$ for $m \in \{x, y, z\}$; $sgn(.)$ is the sign function ; and i is the *iteration index*. Since L_0 and L_1 may never intersect (as they start from opposite endpoints in opposite bones), the JSW $W_k(p)$ can be computed from the tangent field $\vec{N}$ by adding these two optimal lengths yielding a unique value at each voxel p inside R_k (*i.e.*, $\mathrm{W}_k(p) = L_0(p) + L_1(p)$).

IV. Validation

The accuracies of bone motion estimation have been presented in our previous work using DICE score [9]. In this work, we have also quantified the accuracy of joint space area tracking. To do this, we have computed the overlap between automatic (or propagated) and ground-truth (or manual) segmentations of the joint space section at each time frame using the Dice coefficient. The temporal Dice scores across all subjects was around 0.9 ± 0.03, indicating that the joint space area was accurately tracked over the entire ankle trajectory. To validate the accuracy of the implemented Eulerian PDE approach, we have generated a sphere S with center $c = (64, 64, 64)$ and radius $r = 50$ voxels in a regular grid of $128 \times 128 \times 128$ voxels (figure 2) and with an isotropic resolution (voxel size of $1 \times 1 \times 1mm$), under the assumption that the thickness values should be equal to the radius over the sphere. The obtained thickness values inside S using our implementation are effectively around $50.2 \pm 0.4mm$.

V. Results

The tibiotalar JSW is computed in $22sec$ on an Intel® Xeon® Processor E3-1271 v3 3.60 GHz on a $576 \times 576 \times 210$ grid using our optimized implementation of the Eulerian framework (figure 5). The volume of the tracked joint space area increased in the order of maximum dorsiflexion ($183 \pm 10cm^3$), neutral position ($190 \pm 12cm^3$), and maximum plantar flexion ($196 \pm 13cm^3$). Figure 4 shows the estimated JSW values projected on tibial contact surface for several time frames for one subject. It illustrates the temporal evolution of 3D JSW during continuous passive motion for one subject. An advantage of the use of the Eulerian framework is that it yields width values in a bijective way, as shown in the second row in figure 4. From these temporal maps, we can extract temporal features for each subject to provide an average behavior of the JSW. Assuming the central area to be the center of rotation for the tibiotalar joint in healthy feet [4], we define the landmark P_1 shown in figure 3 as the centroid of the joint-space-mesh. For each time-frame for each subject, we then compute the mean average of the JSW inside a sphere centered at P_1 (with radius $r = 20voxels \simeq 5mm$ and by taking into account only the voxels inside the joint space area).

The medial JSW was around $2.7 \pm 0.60mm$ across all healthy ankles throughout the whole motion cycle. The lateral JSW was around $3 \pm 0.60mm$. Obtained measures demonstrate correspondance with the JSW measures presented in [4] for 10 healthy adults from stationary scans. In this work, the authors did not provide any details about the techniques they have used to measure the JSW making it difficult to perform objective comparisons in terms of measurement errors. Figure 3 shows the temporal mean feature of the JSW for all children during the whole ankle trajectory.

In our study, the JSW in the central part (area centred around point $P1$) was not significantly different in any of the positions of the ankle joint while the normal ankle is moving (see Figure 4, thinner orange-yellow areas). In accordance with these results, the ankle moves in this middle position as a centre of rotation for the tibiotalar joint in healthy subjects. This also confirms the results of *Imai et al.* [4] for healthy adults, after dividing the tibial plafond into nine areas. In summary, our methodologies offer many advantages when compared to previous studies such as : reducing the manual interventions as much as possible, tracking the deforming joint space area with high-accuracy, performing 3D width measures over the entire joint space area, in addition to the non-invasive nature of MR imaging.

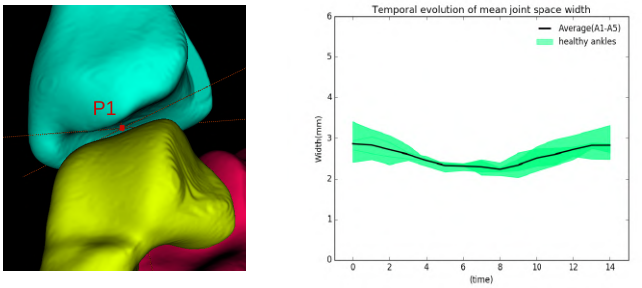

Fig. 3: Temporal evolution of the JSW, from left to right : Location of the centroid of the joint space mesh points (P_1) ; temporal evolution of the JSW around $P1$. The average across subjects is shown as a solid line with one standard deviation above and below this line (grey shaded area).

The source code is available on GitHub : https://github.com/rousseau/dynMRI.

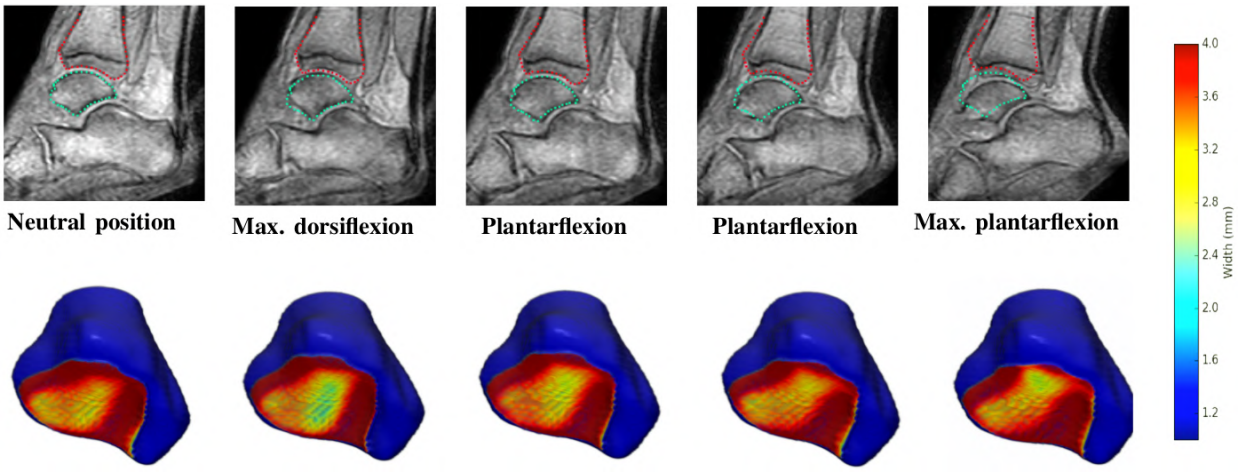

Fig. 4: Spatio-temporal evolution of the tibiotalar JSW during motion. The first row is composed of a set of dynamic anatomical images from one healthy subject : bone contours in neutral position show the joint motion across time (first row). Width values were projected on tibial contact surface (second row).

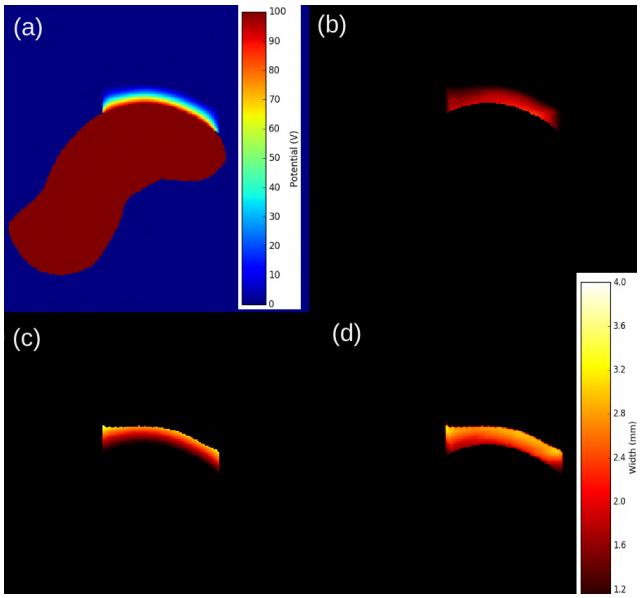

Fig. 5: Calculation of tibiotalar JSW : (a) Harmonic function, (b) Length L_0, (c) Length L_1, (d) width ($L_0 + L_1$).

VI. Conclusion

In this paper, we have presented a complete pipeline for measuring spatio-temporal JSW, providing qualitative visual supports and allowing quantitative data analysis. The proposed approach relying on HR reconstructed dynamic sequences can provide 3D+t morphometric information throughout the whole motion. This work is the first attempt to track the entire joint space area and to evaluate JSWs without having to perform time-consuming manual segmentations. The Eulerian PDE approach provides an efficient and fast solution for quantifying widths of segmented areas, bounded by two bone masks. To conclude, dynamic MRI and dedicated image processing techniques can be applied to study both children and adults with degenerative joint diseases. Moreover, they can eventually be applied to other joints and related muskuloskeletal disorders like the knee OA.

References

[1] D. Hunter, Y. Zhang, X. Tu, M. Lavalley, J. Niu, S. Amin, A. Guermazi, H. Genant, D. Gale, and D. Felson, "Change in joint space width : hyaline articular cartilage loss or alteration in meniscus ?," *Arthritis & Rheumatism : Official Journal of the American College of Rheumatology*, vol. 54, no. 8, pp. 2488–2495, 2006.

[2] A. Burghardt, C. Lee, D. Kuo, S. Majumdar, J. Imboden, T. Link, and X. Li, "Quantitative in vivo HR-pQCT imaging of 3D wrist and metacarpophalangeal joint space width in rheumatoid arthritis," *Annals of Biomedical Engineering*, vol. 41, no. 12, pp. 2553–2564, 2013.

[3] B. Goker, E. Gonen, M. Demirag, and J. Block, "Quantification of the radiographic joint space width of the ankle," *Clinical Orthopaedics and Related Research®*, vol. 467, no. 8, pp. 2083–2089, 2009.

[4] K. Imai, K. Ikoma, M. Kido, M. Maki, H. Fujiwara, Y. Arai, R. Oda, D. Tokunaga, N. Inoue, and T. Kubo, "Joint space width of the tibiotalar joint in the healthy foot," *Journal of Foot and Ankle Research*, vol. 8, no. 1, p. 26, 2015.

[5] B. S. Borotikar and F. T. Sheehan, "In vivo patellofemoral contact mechanics during active extension using a novel dynamic MRI-based methodology," *Osteoarthritis and cartilage*, vol. 21, no. 12, pp. 1886–1894, 2013.

[6] A. Yezzi Jr and J. Prince, "An Eulerian PDE approach for computing tissue thickness," *IEEE Transactions on Medical Imaging*, vol. 22, no. 10, 2003.

[7] O. Acosta, P. Bourgeat, M. Zuluaga, J. Fripp, O. Salvado, S. Ourselin, A. D. N. Initiative, *et al.*, "Automated voxel-based 3D cortical thickness measurement in a combined Lagrangian–Eulerian PDE approach using partial volume maps," *Medical Image Analysis*, vol. 13, no. 5, pp. 730–743, 2009.

[8] J. Fripp, S. Crozier, S. Warfield, and S. Ourselin, "Automatic segmentation and quantitative analysis of the articular cartilages from magnetic resonance images of the knee," *IEEE Transactions on Medical Imaging*, vol. 29, no. 1, pp. 55–64, 2010.

[9] K. Makki, B. Borotikar, M. Garetier, S. Brochard, D. Ben Salem, and F. Rousseau, "High-resolution temporal reconstruction of ankle joint from dynamic MRI," in *IEEE ISBI*, pp. 1297–1300, 2018.

[10] V. Arsigny, O. Commowick, N. Ayache, and X. Pennec, "A fast and log-euclidean polyaffine framework for locally linear registration," *Journal of Mathematical Imaging and Vision*, vol. 33, no. 2, pp. 222–238, 2009.

[11] K. Makki, B. Borotikar, M. Garetier, S. Brochard, D. B. Salem, and F. Rousseau, "In vivo ankle joint kinematics from dynamic magnetic resonance imaging using a registration-based framework," *Journal of biomechanics*, vol. 86, pp. 193–203, 2019.